Coexistence of ferroelectric vortex domains and charged domain walls in epitaxial BiFeO3 film on (110)O GdScO3 substrate

Qi, Yajun; Chen, Zuhuang; Huang, Chuanwei; Wang, Lihua; Han, Xiaodong; Wang, Junling; Yang, Ping; Sritharan, Thirumany; Chen, Lang

2012

Qi, Y., Chen, Z., Huang, C., Wang, L., Han, X., Wang, J., et al. (2012). Coexistence of ferroelectric vortex domains and charged domain walls in epitaxial BiFeO3 film on (110)O GdScO3 substrate. Journal of Applied Physics, 111(10), 104117-.

https://hdl.handle.net/10356/94819

https://doi.org/10.1063/1.4722253

AIP | Journal of Applied Physics

Coexistence of ferroelectric vortex domains and charged domain walls in epitaxial BiFeO3 film on (110)O GdScO3 substrate

Yajun Qi, Zuhuang Chen, Chuanwei Huang, Lihua Wang, Xiaodong Han et al.

Citation: J. Appl. Phys. **111**, 104117 (2012); doi: 10.1063/1.4722253
View online: http://dx.doi.org/10.1063/1.4722253
View Table of Contents: http://jap.aip.org/resource/1/JAPIAU/v111/i10
Published by the American Institute of Physics.

Coexistence of ferroelectric vortex domains and charged domain walls in epitaxial $BiFeO_3$ film on $(110)_O$ $GdScO_3$ substrate

Yajun Qi,[1,2] Zuhuang Chen,[1] Chuanwei Huang,[1] Lihua Wang,[3] Xiaodong Han,[3] Junling Wang,[1] Ping Yang,[4] Thirumany Sritharan,[1] and Lang Chen[1,a)]
[1]*School of Materials Science and Engineering, Nanyang Technological University, Singapore 639798, Singapore*
[2]*Department of Materials Science and Engineering, Hubei University, Wuhan 430062, People's Republic of China*
[3]*Institute of Microstructure and Properties of Advanced Materials, Beijing University of Technology, Beijing 100022, People's Republic of China*
[4]*Singapore Synchrotron Light Source (SSLS), National University of Singapore, 5 Research Link, Singapore 117603, Singapore*

(Received 27 April 2012; accepted 27 April 2012; published online 30 May 2012)

The occurrence of ferroelectric charged domain walls (CDWs) which was thought to be energetically unstable is observed, together with a ferroelectric vortex structure composed of 109° and 180° domains near an epitaxial $BiFeO_3/GdScO_3$ interface. The CDW and vortex affect the domain arrangement, domain configuration, and hence tune the domain size distribution. © *2012 American Institute of Physics*. [http://dx.doi.org/10.1063/1.4722253]

I. INTRODUCTION

The "ferrotoroidal" ordering in ferromagnetic and ferroelectric materials is currently a subject of intensive interest due to the intriguing fundamental physics and the potential applications.[1–12] Unlike in ferromagnets,[1–3] the existence of vortex domain structures in ferroelectrics is less well established, despite being theoretically predicted several years ago.[4,5] Some recent experimental works have provided credible evidences for their existence.[6–12] Analogous to spin arrangement in ferromagnetics, the local electrical dipoles in nanometer scale ferroelectric structures are likely to arrange themselves in vortices due to the large depolarization field.[4,5] Recent works are beginning to shed light on the prevalence and stability of ferroelectric dipole closure phenomenon in nanoscale structures as follows: (i) formation of flux-closure quadrant domains in single crystal lamellae and nanodots of $BaTiO_3$;[6–8] (ii) formation of small-scale flux-closure states in $BiFeO_3$ (BFO) films by direct writing using scanning probe tips; and [9,10] (iii) observation of vortex structures in $Pb(Zr_{0.4}Ti_{0.6})O_3$ (PZT) nanodots[11] and $Pb(Zr_{0.3}Ti_{0.7})O_3$ fine-grained polycrystalline samples.[12]

Most reports were based on interpretations of piezoresponse force microscopy (PFM) images, where the vortex polarization states were indirectly detected by the contrast at the junction between two sets of 90° domain walls or four segments of different domain patterns.[8–12] The spatial resolution of PFM is limited by the probe tip radius. It does not allow detail characterization of the core of the closure structures underneath the tip beyond the radius of the tips. With the advent of high resolution, aberration-corrected cross-sectional transmission electron microscopy (Cs-TEM), continuous rotation of the dipoles closing the flux of 180° domains was directly observed in a $PbZr_{0.2}Ti_{0.8}O_3$ thin film recently.[13] Vortex nanodomains near the interface between a BFO film and the $TbScO_3$ substrate was also detected in electric polarization mapping using a Cs-scanning TEM.[14] The triangle-shaped vortex domains consist of a mirrored pair of inclined 180° domain walls, which form a vortex domain structure with the polarization rotating about the intersection of two 109° and two 180° domain walls. Formation of such vortex domains is an effective way to further minimize the local depolarization field energy[14] near the film-substrate interface, in addition to the prevailing existence of 109° domains that can screen the depolarization field macroscopically.

In the vortex domains, dipoles rotate continuously forming a flux-closure pattern, which is unlike the common "head-to-tail" arrangement across a domain boundary. Interestingly, a recent calculation suggested that a head-to-head or a tail-to-tail configuration could be energetically favorable if the poling ability of the surface is large enough.[15] Although, such boundaries carrying net charges are energetically unstable, they have been observed in some ferroelectrics, such as in $Ca_{0.28}Ba_{0.72}Nb_2O_6$ single crystals,[16] La doped $Pb[Zr_xTi_{1-x}]O_3$ ceramics[17] and PZT,[18] and BFO thin films.[19,20] The existence of charged domain walls (CDWs) will affect the domain size and configuration, and its physical and electrical properties such as switching and conducting. For instance, a very recent report shows that the CDWs lower the local energy bandgap and thus enhances the photocurrent.[20] In this paper, we report the existence of a vortex domain structure as well as stable CDWs in a BFO film grown by pulsed laser deposition on $(110)_o$ $GdScO_3$ (GSO) substrate belonging to the space group *Pbnm* with lattice constants $a_o = 5.488$ Å, $b_o = 5.746$ Å, and $c_o = 7.934$ Å.[21] Herein and after, subscripts "*c*" and "*o*" denote the pseudocubic and orthorhombic crystal structures, respectively. The $(110)_o$-oriented GSO substrate has anisotropic in-plane

a)Author to whom correspondence should be addressed. Electronic mail: langchen@ntu.edu.sg.

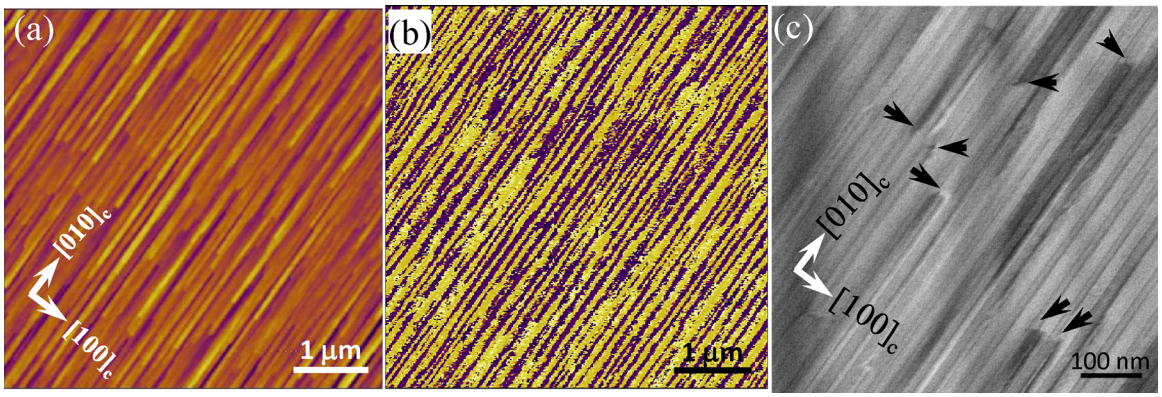

FIG. 1. AFM topography (a), out-of-plane PFM image (b), plan-view bright-field TEM image (c) of a BFO film on $(110)_o$ $GdScO_3$ substrate. The arrows in (c) indicated the domain intersections.

lattice of $a_c = 3.967$ Å and $b_c = 3.973$ Å and with a very small lattice mismatch (~0.1%) with BFO. The periodicity of the 109° domains was measured by synchrotron x-ray, and by plan-view and cross-sectional TEM investigations. The arrangement of the polarization for each domain as well as the CDWs was determined using dark-field image technique in the TEM.

II. EXPERIMENTAL RESULTS

BFO films were deposited on $(110)_o$ GSO single crystal substrates by pulsed laser deposition. Details of the deposition, the atomic force microscopy (AFM), and synchrotron x-ray diffraction (XRD) procedures are described elsewhere.[22,23] The reciprocal space mappings (RSM) are plotted in reciprocal lattice units of the GSO substrate defined by the monoclinic unit cell (1 r.l.u. = 3.967 $Å^{-1}$ for H direction, 1 r.l.u. = 3.973 $Å^{-1}$ for L direction). The reciporcal space coordinate H, K, and L are directions along $[001]_o$, $[\bar{1}10]_o$, and $[110]_o$, respectively. Plan-view and cross-sectional TEM specimens were prepared using the standard procedure consisting of cutting, gluing, mechanical polishing, and ion milling. TEM investigations were carried out on JEOL electron microscopes JEM2100F (FEG) and Tecnai G20 operated at 200 kV.

X-ray diffraction θ–2θ scan confirmed that the films are pure BFO. Figure 1(a) shows the typical "puckered" topography of the BFO thin film surface with a root mean square roughness of 0.7 nm. The out-of-plane PFM phase image (Fig. 1(b)) shows essentially a stripe-like contrast throughout the film. This "puckered" surface and the domain structure correspond to the washboard-like schematic of 109° domain configuration, consistent with the previous studies.[24–26] The alternating yellow and purple contrast in Fig. 1(b) signifies a corresponding change in the out-of-plane component of the polarization vector, which is consistent with the interpretation of a 109° rotation of the polarization vector across the wall. Fig. 1(c) shows a typical plan-view, bright-field TEM image of the film. A stripe-like parallel domain structure aligned to the $[010]_c$ (or $[\bar{1}10]_o$) direction is clear. The width of the domains approximately ranges from 6 nm to 30 nm, with the most probable width of a single domain centered around 10 to 17 nm. In addition, one can also see some domain intersections marked by arrows in the figure, which may correspond to 180° domain walls or CDWs as will be elaborated subsequently.

The periodic stripe domains were also confirmed by synchrotron RSMs. Fig. 2 shows the specular RSMs on $(002)_c$ (or $(220)_o$) and reflection of the same film within the scattering zone (H0L) and (HK0). In addition to the main reflections for the film and the substrate, extra superlattice spots

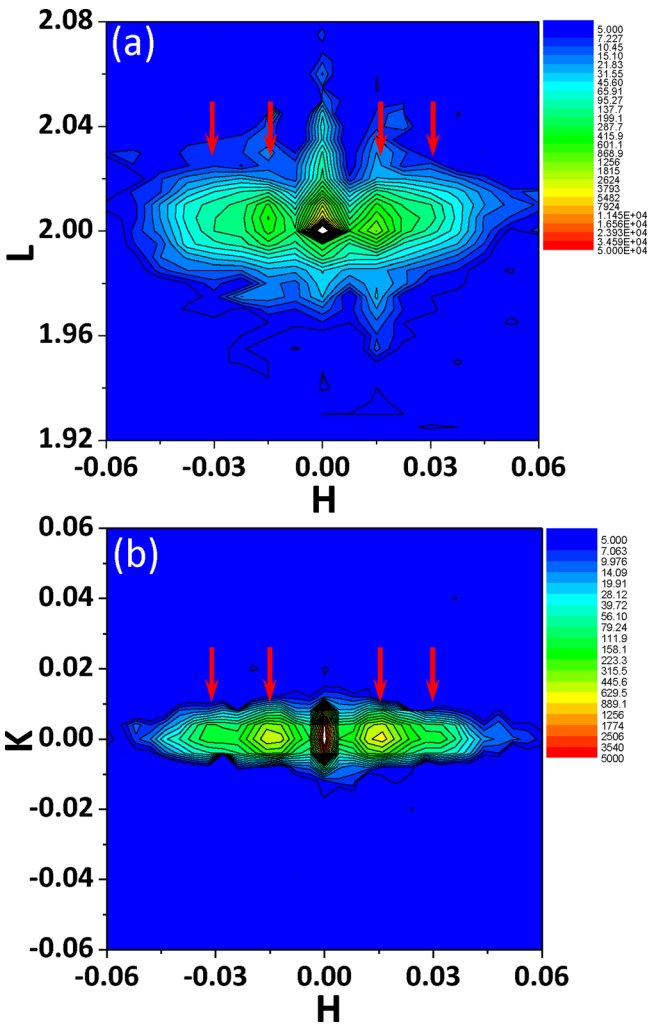

FIG. 2. Synchrotron RSMs near $(220)_o$ reflection taken in HL (a) and HK (b) spaces of a BFO film on GSO substrate.

corresponding to the periodic domain structure can be seen clearly adjacent to the main $(220)_o$ Brag reflection in both HL and HK spaces. As indicated by arrows, two sets of the satellite peaks with an interval of $\Delta H = 0.016$ are apparent. The spacing of these satellite peaks approximately correspond to a domain periodicity of ~25 nm.

Figures 3(a) and 3(b) show a pair of dark-field TEM images of the same area close to the zone axis $[\bar{1}10]_o$, taken with near two beams $\mathbf{g} = 110_o$ and $\mathbf{g} = \bar{1}\bar{1}0_o$ (or $\mathbf{g} = 001_c$ and $\mathbf{g} = 00\bar{1}_c$), respectively. The thickness of the film is estimated as 24 nm. The alternating dark and bright contrasts show the domain structure of the film. Three types of domains can be identified: (i) stripe domains with $(100)_c$ vertical domain walls, (ii) 180° domains with $(101)_c$ domain walls, and (iii) triangle vortex nanodomains (indicated by arrows). The statistics of the measured width of 109° domains is shown in Fig. 3(e), where sample size is 134. The width ranges from 6 nm to 30 nm, with the mode at ~11 nm; the most probable width of a single domain is centered at 10 to 16 nm which indicates that the periodicity of the 109° domains is 20–32 nm, in agreement with the plan-view TEM and RSMs results. Note that the domain size distribution is not symmetrical about the mode at 11 nm but is skewed towards the large domain sizes with a long tail. Consequently, the mean (average), 14.5 nm) is larger than the median, 13 nm; and both are larger than the single mode, 11 nm. The statistical results of domain width caution us against the use of a single parameter (mode, average, or median) to describe the domain width's complex distribution. It also challenges the understanding derived from phenomenological mean-field scaling without consideration of the actual, strongly asymmetrical distribution of domain width.

Figure 3(f) gives the selected area electron diffraction (SAED) patterns obtained at the film-substrate interface. The patterns were indexed on the basis of the pseudo-cubic and orthorhombic unit cell of BFO and GSO, respectively. The splitting of spots evident in the high-order diffraction spots could be attributed to the small misfit between the film and substrate lattice parameters, and the high quality of epitaxy of the film. From the SAED patterns, the orientation relationship of the film and the substrate can be determined to be $(001)_c$ BFO//$(110)_o$ GSO and $[010]_c$ BFO//$[\bar{1}10]_o$ GSO.

However, when the film was viewed along $[001]_o$ (or $[100]_c$) direction, which is 90° with respect to $[\bar{1}10]_o$ direction, it exhibited uniform contrast signifying the absence of any domain patterns, as shown in Fig. 3(d). This indicates that the film consist of two ferroelastic domains which is in agreement with previous studies.[14,26] The SAED pattern (Fig. 3(g)) along $[001]_o$ zone axis also proves the high epitaxy of the film.

The direction of the polarization vector in each ferroelectric domain can be determined using the dark-field technique under two-beam condition. In this technique, a domain with a polarization vector $\mathbf{P}$ gives a bright contrast for $\mathbf{g} \cdot \mathbf{P} > 0$, where $\mathbf{g}$ is a scattering vector.[27–29] In Figs. 3(a) and 3(b) images with $\mathbf{g} = 001_c$ and $\mathbf{g} = 00\bar{1}_c$, the bright and dark

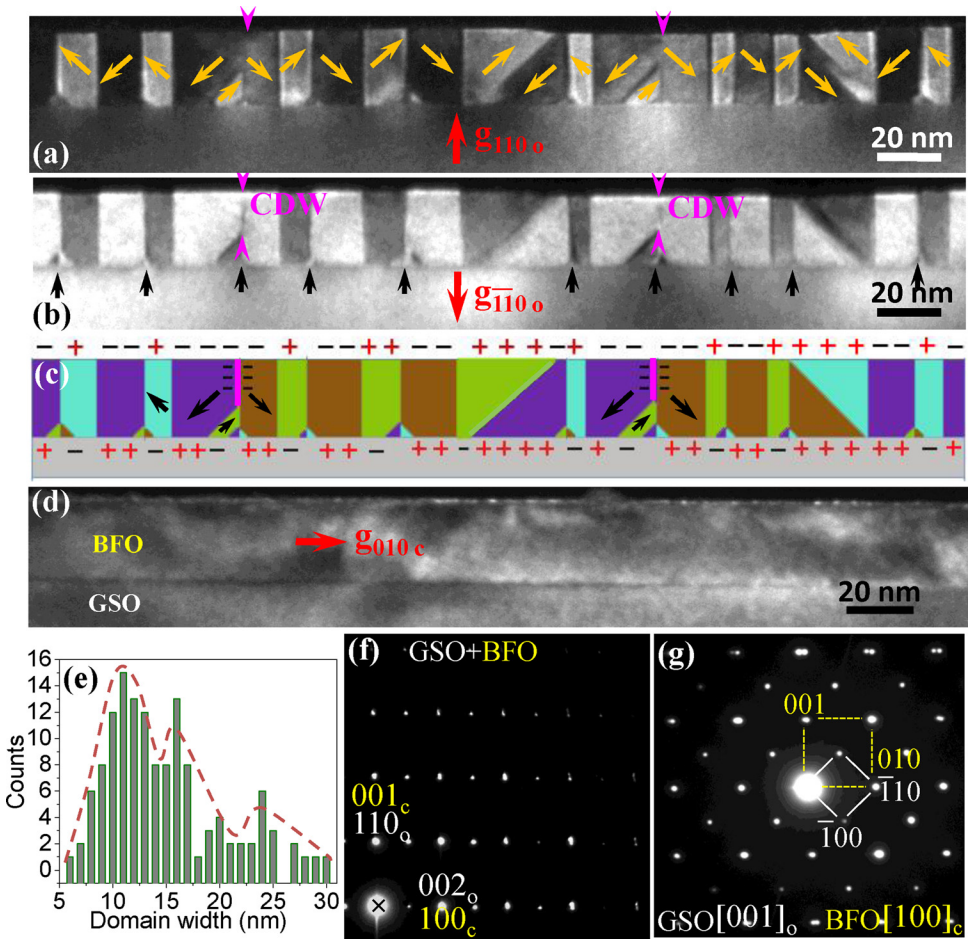

FIG. 3. Dark-field TEM images of the same area close to the zone axis $[\bar{1}10]_o$, taken with near two beam $\mathbf{g} = 110_o$ (a) and $\mathbf{g} = \bar{1}\bar{1}0_o$ (b); (c) a schematic of domain structures in (a) and (b); (d) dark-field image near $[001]_o$ zone axis using $\mathbf{g} = 010_c$ (or $\bar{1}10_o$); a histogram of a single domain width distribution (e) and the SAED pattern along $[\bar{1}10]_o$ (f) and $[001]_o$ (g) from the interface between the substrate and the film. Yellow arrows denote the polarization directions in (a).

contrasts are perfectly reversed. This proves that the bright contrast regions in Figs. 3(a) and 3(b) have polarization components parallel to the $[001]_c$ and $[00\bar{1}]_c$ directions, respectively. It is already proven in the $(001)_c$ BFO films on the $(110)_o$ rare-earth scandate substrate that only two ferroelastic structural variants with spontaneous polarizations rotated by 109° exist in adjacent domains.[26] With these two critical pieces of information, the polarization direction in each domain can be derived as indicated by the arrows in Fig. 3(a). The electric charges accumulating at the interfaces could also be derived from the polarization directions as shown in Fig. 3(c). Unexpectedly, a tail-to-tail configuration or CDWs with net negative charges were obtained near the top surface as indicated by purple arrows (Figs. 3(a) and 3(b)) and lines (Fig. 3(c)), even though self-consistency of the polarization arrangement has been taken into consideration.

Interestingly, the CDWs exist only near the top free surface and intersect with the half threading 180° domain walls. While in the area with 180° domain walls penetrating from the film-substrate interface to the top surface, no CDW was observed. This can be explained by domain wall energy consideration. In the local area with absorbed charges at the top surface of the film,[30] the 180° domain walls may not be energetically favorable if they penetrate through the whole film since the 180° domain wall has the highest wall energy among the three possible domain walls of 71°, 109°, and 180° in BFO.[31]

High resolution TEM (HRTEM) images of Figs. 4(a) and 4(b) show coherency across the boundaries near the vertical domain walls, charged domain wall, and the triangle vortex nanodomain. According to the polarization arrangement shown in Fig. 3(a), the direction of the triangle domain can be deduced, as indicated by the arrows. No deviation is observed across the CDW indicated by purple arrows. If you consider a vertical 109° domain wall at a triangular vortex, it is clear that it splits into a mirrored pair of inclined 180° domain walls and a 109° domain wall of opposite sense. In fact, the continuous polarization at these triangular areas rotate about the intersection of two 109° and two 180° domain walls forming a vortex domain structure.[14]

III. DISCUSSION AND CONCLUSION

The appearance of the vortex domains and the CDWs provide additional compensation of depolarization field energy and closely correlate with the depolarization field, domain walls, or even the unavoidable screening charges from adsorbed species. This will result in different domain size and configuration compared with the one without CDWs. The introduction of vortex domains and CDWs contributes to the asymmetric electrostatic boundary condition, as described in our previous work,[32,33] which strongly affects the domain size, even the domain type, and deviates the domain scaling mechanism from the classical Kittel's law.[34] The bound charges near the CDWs change the local electrostatic field and the domain structure. These local effects make the domain structure complex and, as a consequence, a strongly asymmetrical domain size distribution was observed in Fig. 3(e). On the other hand, the mode of 11 nm from the statistic results

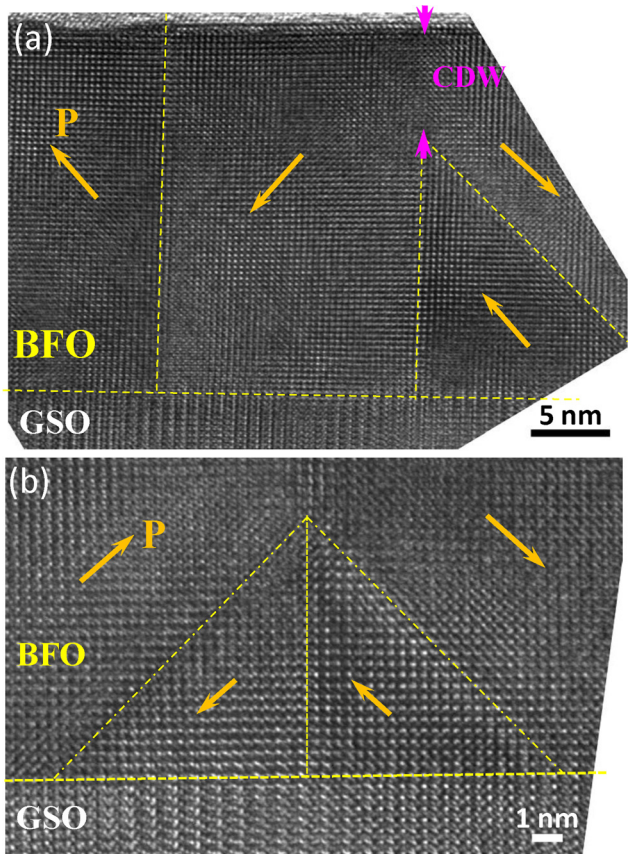

FIG. 4. HRTEM images near the boundaries of the 109° and 180° domains (a) and the vortex nanodomain (b) with the GSO surface. Yellow arrows indicate polarization direction, purple arrows highlight the charged domain wall, and dashed lines indicate the position of the domain walls.

(Fig. 3(e)) is in agreement with the measurements made by a synchrotron XRD, which is a global macroscopic detecting technique where the local structural information is averaged.

The coexistence of the vortex domains and CDWs will not only affect the domain structure but also affect the physical properties of the films. The CDWs with bound charges could be the pinning centers for domain switching and could lead to fatigue and imprint problems in information storage applications. Furthermore, it could also lower local energy bandgap of the film[20] and improve photon absorption in photovoltaic applications.

In summary, the coexistence of CDWs and vortex structures in a thin ferroelectric film composed of 109° and 180° domains near an epitaxial BFO/GSO interface were revealed by TEM. The periodicity of ~25 nm of the stripe 109° domain was confirmed both by synchrotron RSM and the mode of the statistical results of width measurements from TEM images. Triangle vortex domains and CDWs were clearly identified in dark-field TEM images. The coexistence of the CDWs and the vortex domain results in a wide distribution of the domain size properties of the film.

ACKNOWLEDGMENTS

We acknowledge the support from the Singapore National Research Foundation under its CREATE program: Nanomaterials for Energy and Water Management.

[1]T. Shinjo, T. Okuno, R. Hassdorf, K. Shigeto, and T. Ono, Science **289**, 930 (2000).
[2]A. Wachowiak, J. Wiebe, M. Bode, O. Pietzsch, M. Morgenstern, and R. Wiesendanger, Science **298**, 18 (2002).
[3]S.-B. Choe, Y. Acremann, A. Scholl, A. Bauer, A. Doran, J. Stohr, and H. A. Padmore, Science **304**, 420 (2004).
[4]I. I. Naumov, L. Bellaiche, and H. Fu, Nature **432**, 737 (2004).
[5]H. Fu and L. Bellaiche, Phys. Rev. Lett. **91**, 257601 (2003).
[6]A. Schilling, D. Byrne, G. Catalan, K. Weber, Y. Genenko, G. Wu, J. F. Scott, and J. M. Gregg, Nano Lett. **9**, 3359 (2009).
[7]L. J. McGilly, A. Schilling, and J. M. Gregg, Nano Lett. **10**, 4200 (2010).
[8]R. G. P. McQuaid, L. J. McGilly, P. Sharma, A. Gruverman, and J. M. Gregg, Nat. Commun. **2**, 404 (2011).
[9]N. Balke, S. Choudhury, S. Jesse, M. Huijben, Y. H. Chu, A. P. Baddorf, L. Q. Chen, R. Ramesh, and S. V. Kalinin, Nat. Nanotechnol. **4**, 868 (2009).
[10]R. K. Vasudevan, Y. C. Chen, H. H. Tai, N. Balke, P. P. Wu, S. Bhattacharya, L. Q. Chen, Y. H. Chu, I. N. Lin, S. V. Kalinin, and V. Nagarajan, ACS Nano **5**, 879 (2011).
[11]B. J. Rodriguez, X. S. Gao, L. F. Liu, W. Lee, I. I. Naumov, A. M. Bratkovsky, D. Hesse, and M. Alexe, Nano Lett. **9**, 1127 (2009).
[12]Y. Ivry, D. P. Chu, J. F. Scott, and C. Durkan, Phys. Rev. Lett. **104**, 207602 (2010).
[13]C. L. Jia, K. W. Urban, M. Alexe, D. Hesse, and I. Vrejoiu, Science **331**, 1420 (2011).
[14]C. T. Nelson, B. Winchester, Y. Zhang, S. J. Kim, A. Melville, C. Adamo, C. M. Folkman, S. H. Baek, C. B. Eom, D. G. Schlom, L. Q. Chen, and X. Q. Pan, Nano Lett. **11**, 828 (2011).
[15]M. Y. Gureev, A. K. Tagantsev, and N. Setter, Phys. Rev. B **83**, 184104 (2011).
[16]C. J. Lu, C. J. Nie, X. F. Duan, J. Q. Li, H. J. Zhang, and J. Y. Wang, Appl. Phys. Lett. **88**, 201906 (2006).
[17]C. A. Randall, D. Barber, and R. W. Whatmore, J. Mater. Sci. **22**, 925 (1987).
[18]C. L. Jia, S.-B. Mi, K. Urban, I. Vrejoiu, M. Alexe, and D. Hesse, Nature Mater. **7**, 57 (2008).
[19]N. Balke, M. Gajek, A. K. Tagantsev, L. W. Martin, Y. H. Chu, R. Ramesh, and S. V. Kalinin, Adv. Funct. Mater. **20**, 3466 (2010).
[20]W. M. Lee, J. H. Sung, K. Chu, X. Moya, D. Lee, C. J. Kim, N. D. Mathur, S.-W. Cheong, C.-H. Yang, and M. H. Jo, Adv. Mater. **24**, OP49 (2012).
[21]S. Geller, Acta Crystallogr. **10**, 243 (1957).
[22]Z. H. Chen, L. You, C. W. Huang, Y. J. Qi, J. L. Wang, T. Sritharan, and L. Chen, Appl. Phys. Lett. **96**, 252903 (2010).
[23]Z. H. Chen, Z. L. Luo, C. W. Huang, Y. J. Qi, P. Yang, L. You, C. S. Hu, T. Wu, J. L. Wang, C. Gao, T. Sritharan, and L. Chen, Adv. Funct. Mater. **21**, 133 (2011).
[24]S. K. Streiffer, C. B. Parker, A. E. Romanov, M. J. Lefevre, L. Zhao, J. S. Speck, W. Pompe, C. M. Foster, and G. R. Bai, J. Appl. Phys. **83**, 2742 (1998).
[25]Y. H. Chu, Q. He, C. H. Yang, P. Yu, L. W. Martin, P. Shafer, and R. Ramesh, Nano Lett. **9**, 1726 (2009).
[26]C. M. Folkman, S. H. Baek, H. W. Jang, C. B. Eom, C. T. Nelson, X. Q. Pan, Y. L. Li, L. Q. Chen, A. Kumar, V. Gopalan, and S. K. Streiffer, Appl. Phys. Lett. **94**, 251911 (2009).
[27]M. Tanaka and G. Honjo, J. Phys. Soc. Jpn. **19**, 951 (1964).
[28]F. J. Fujimoto, J. Phys. Soc. Jpn. **14**, 1558 (1959).
[29]T. Asada and Y. Koyama, Phys. Rev. B **75**, 214111 (2004).
[30]D. D. Fong, A. M. Kolpak, J. A. Eastman, S. K. Streiffer, P. H. Fuoss, G. B. Stephenson, C. Thompson, D. M. Kim, K. J. Choi, C. B. Eom, I. Grinberg, and A. M. Rappe, Phys. Rev. Lett. **96**, 127601 (2006).
[31]A. Lubk, S. Gemming, and N. A. Spaldin, Phys. Rev. B **80**, 104110 (2009).
[32]C. W. Huang, L. Chen, J. Wang, Q. He, S. Y. Yang, Y. H. Chu, and R. Ramesh, Phys. Rev. B **80**, 140101 (2009).
[33]C. W. Huang, Z. H. Chen, J. L. Wang, T. Sritharan, and L. Chen, J. Appl. Phys. **110**, 014110 (2011).
[34]C. Kittel, Phys. Rev. **70**, 965 (1946).